Supplementary Information

Plasma-Driven Redox mechanism in the Reverse Water–Gas Shift Reaction over Ni–In intermetallic catalysts

Dae-Yeong Kim[a*], Zhang Wenjun[a], Kaiyue Dong[b], Bang Lu[b], Duanxing Li[c], Satoru Takakusagi[b], Shinya Furukawa[c], and Tomohiro Nozaki[a]

[a]Department of Mechanical Engineering, Institute of Science Tokyo, Tokyo 152-8550, Japan

[b]Institute for Catalysis, Hokkaido University, Sapporo 001-0021, Japan

[c]Division of Applied Chemistry, Osaka University, Osaka 565-0871, Japan

[*]Corresponding authors. Email: kim.d.as@m.titech.ac.jp (D-Y.K.)

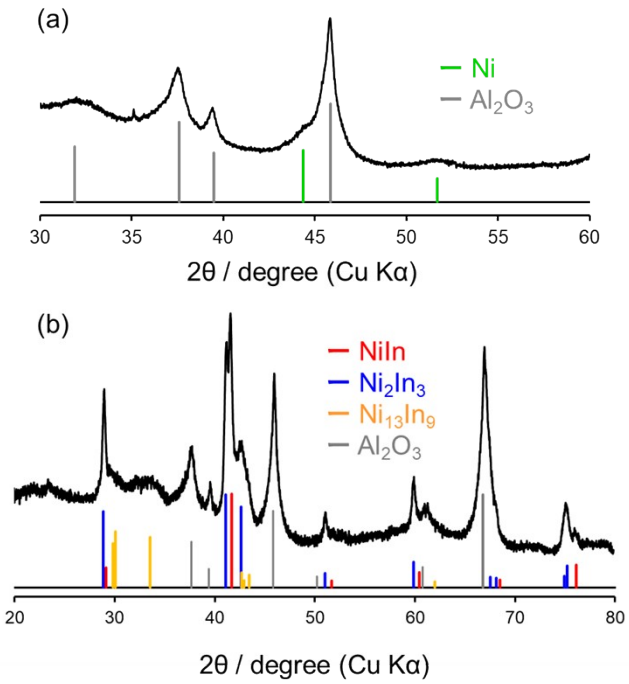

Figure S1. X-ray diffraction patterns of (a) Ni and Ni–In/Al_2O_3. Colored vertical lines indicate the references for the corresponding phases. By using the Scherrer's equation, the crystallize sizes of Ni and Ni–In nanoaprticles were estimated as 6 and 16 nm, respectively.

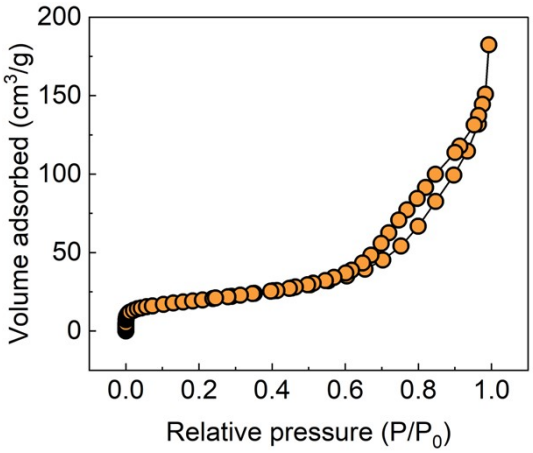

Figure S2. N_2 adsorption-desorption isotherms of Ni–In/Al_2O_3.

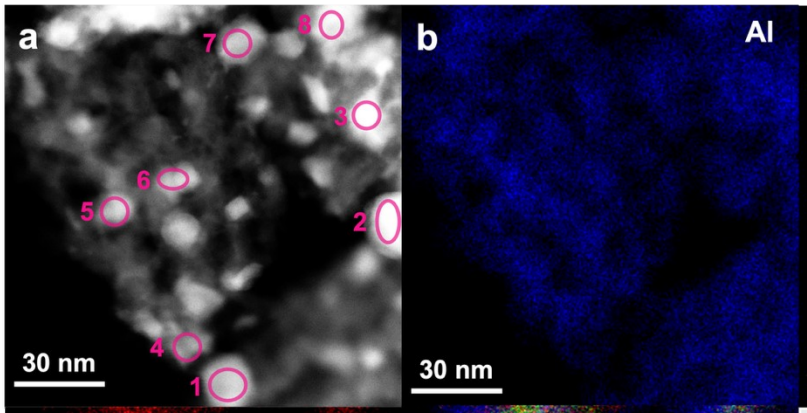

Position	Ni/In molar ratios
1	1.2
2	1.2
3	1.1
4	1.1
5	1.0
6	1.3
7	1.3
8	1.5

Figure S3. TEM analysis of the Ni–In/Al_2O_3 catalyst. (a) HAADF-STEM image and corresponding elemental maps of (b) Al, (c) Ni, (d) In, and (e) an overlay of Al, Ni, and In. The Ni/In molar ratios at the positions marked with pink circles in (e) are summarized in the table on the right.

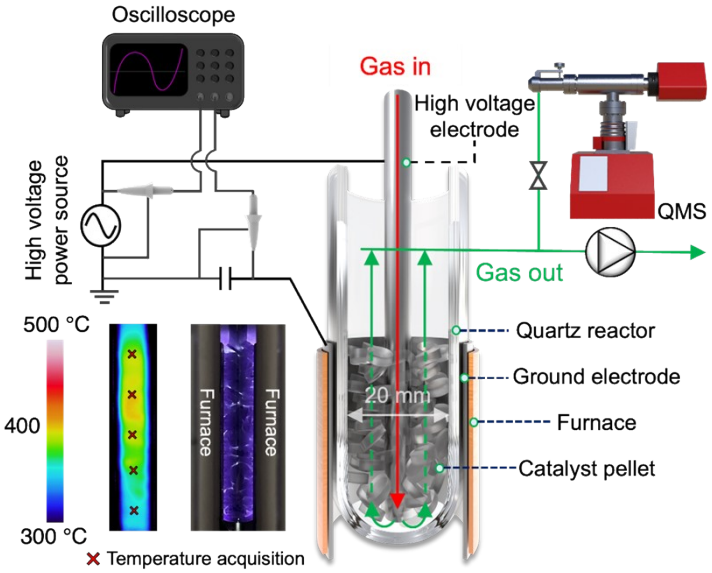

Figure S4. Schematic diagram of the detailed setup of the packed-bed DBD reactor.

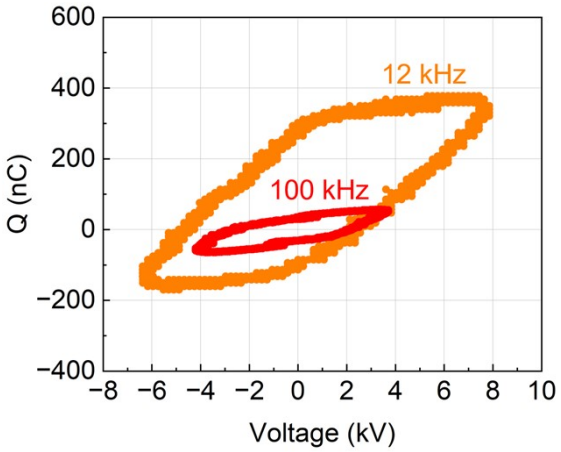

Figure S5. Lissajous figures for plasma discharges at 12 kHz and 100 kHz

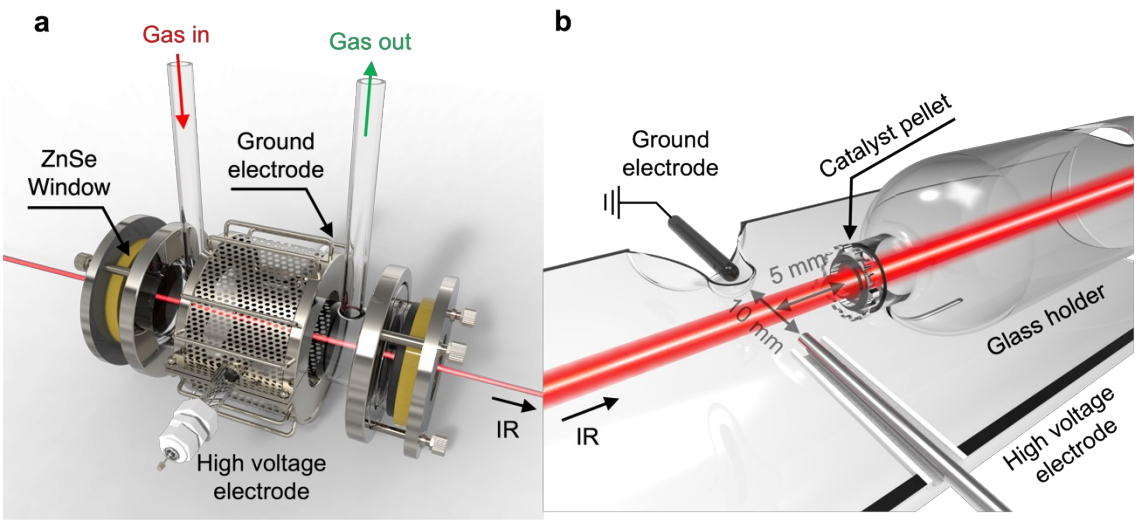

Figure S6. Schematic diagram of the *in situ* TIR cell (a) and the electrode and catalyst pellet geometry (b). The ZnSe windows were replaced with Kapton film (polymide) when *in situ* XAFS was employed.

Supplementary Note 1. Kinetic analysis

Kinetic analyses were conducted under a kinetically controlled regime (the CO_2 conversion was lower than 20 %) by adjusting the WHSV to 6000 $cm^3/g/h$ (Figure S7). CO reaction rate was expressed by the power-law kinetics (Eq. (1)). Take the natural logarithm of Eq. (1) and rewrite it into Eqs. (2) - (4):

$$-\frac{dP_{CO}}{dt} = r_{CO} = kP_{CO_2}{}^{\alpha}P_{H_2}{}^{\beta} \quad (1)$$

$$r_{CO} = \ln k + \alpha \ln P_{CO_2} + \beta \ln P_{H_2} \quad (2)$$

$$ln\frac{r_{CO}}{P_{H_2}{}^{\beta}} \propto \alpha\, lnP_{CO_2} \quad (3)$$

$$ln\frac{r_{CO}}{P_{CO_2}{}^{\alpha}} \propto \beta\, lnP_{H_2} \quad (4)$$

Here, k and P expresses the reaction rate constant and the average concentration of CO_2 and H_2. α and β represent the modified reaction order for CO_2 and H_2, respectively. α and β were unknown figures at this point: Assume arbitrary values for α and β and performed iterative calculations until the deviation of α and β becomes smaller than 1% error. The feasibility of this method had been verified by comparing with conventional approach with inert gas dilution in our previous research on dry methane reforming.[1]

Reaction order was estimated from Figure S8 at fixed total flow rate while varying H_2/CO_2 ratio without dilution gas. Figure S9 represents the corresponding CO_2 and H_2 conversion and CO selectivity. Experimental conditions are provided in the figure caption of Figure S9. In Figure S8a and S8b, $ln\frac{r_{CO}}{P_{H_2}{}^{\beta}}$ v.s. $\ln P_{CO_2}$ and $ln\frac{r_{CO}}{P_{CO_2}{}^{\alpha}}$ v.s. $\ln P_{H_2}$ express the linear relationship.

Apparent activation energy (E_A) under thermal and DBD conditions was determined according to Eqs. (1) and (5):

$$k = Ae^{-\frac{E_A}{RT}} \quad (5)$$

The A, R and T represent pre-exponential factor, universal gas constant and catalyst temperature (K), respectively.

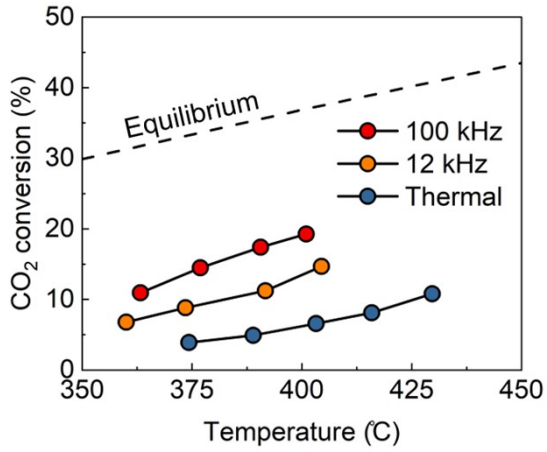

Figure S7. Temperature-dependent CO_2 conversion. Reaction conditions: Total flow rate = 800 mL/min (STP); H_2/CO_2 = 3; WHSV 6000 mL/g/h (STP); pressure = 30 kPa; SEI =1.5 eV/molecules.

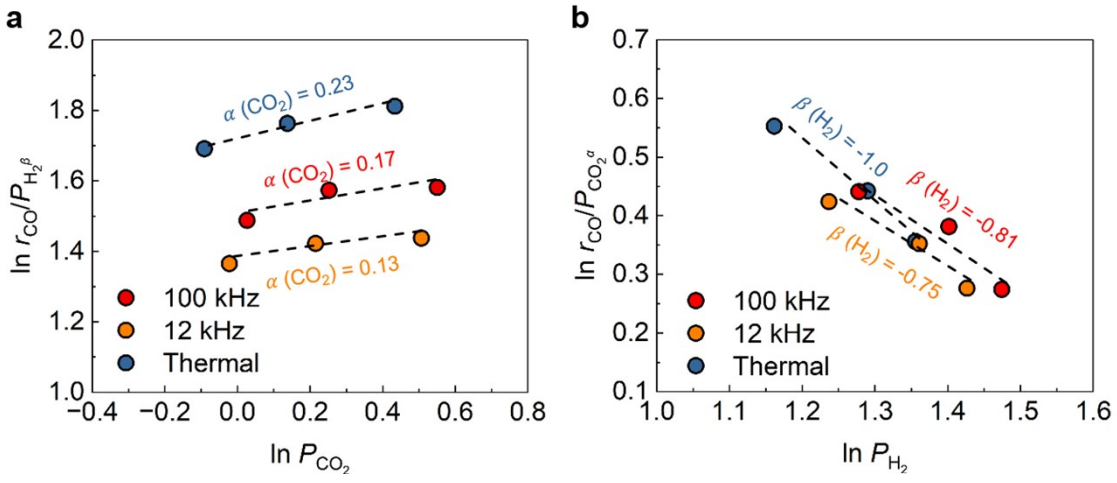

Figure S8. Reaction orders (a) α for CO_2 and (b) β for H_2. Conditions: see Figure S9 caption.

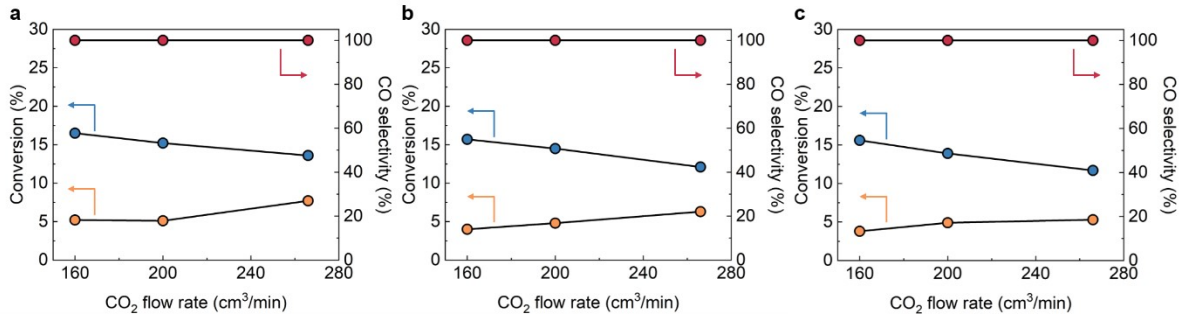

Figure S9. CO_2 and H_2 conversion with respect to the CO_2 flow rate over Ni-In/Al_2O_3. (a) Thermal, (b) 12 kHz DBD and (c) 100 kHz DBD conditions. Reaction conditions: Catalyst temperature = 450 °C (Thermal), 380 °C (12 kHz DBD) and 410 °C (100 kHz DBD); Total flow rate = 800 mL/min (STP); H_2/CO_2 = 2, 3 and 4; WHSV = 6000 mL/g/h (STP); pressure = 30 kPa; SEI =1.5 eV/molecules.

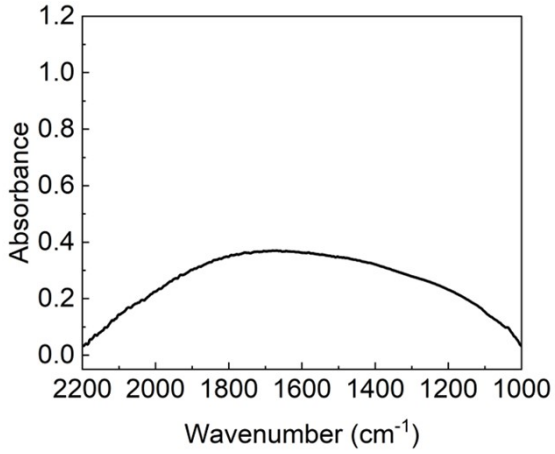

Figure S10. *In situ* TIR spectra of Ni-In/Al_2O_3 recorded at 350 °C under O_2 exposure.

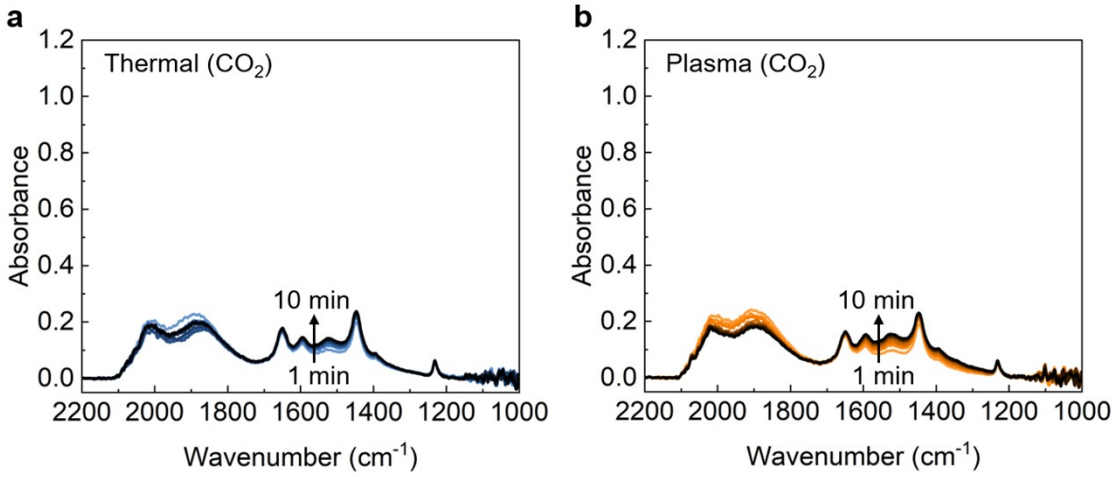

Figure S11. *In situ* TIR spectra of Ni/Al_2O_3 recorded at 350 °C during CO_2 exposure under (a) thermal and (b) DBD conditions.

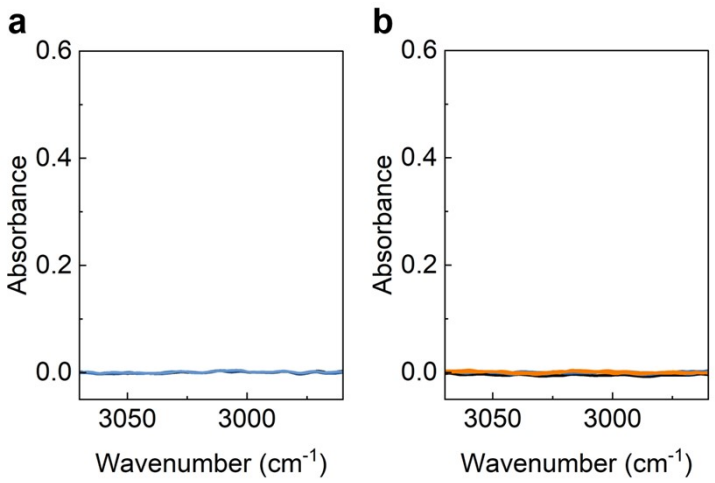

Figure S12. *In situ* TIR spectra of CH_4 peak area at 3015 cm^{-1} corresponding to (a) Figure 2c and (b) Figure 2d in main text.

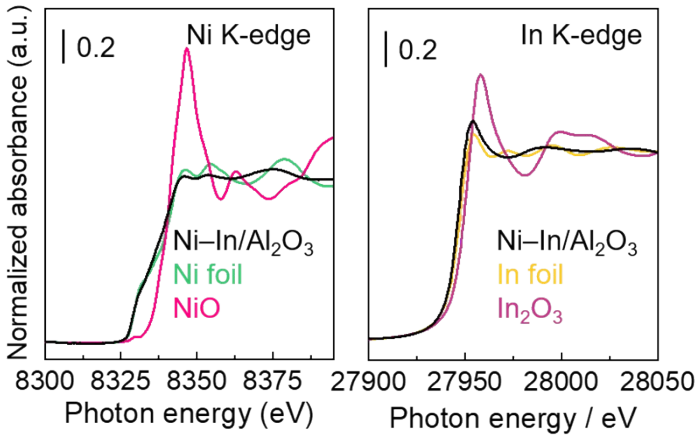

Figure S13. *In situ* Ni and In K-edge XANES spectra of Ni–In/Al_2O_3 collected at room temperature after reduction.

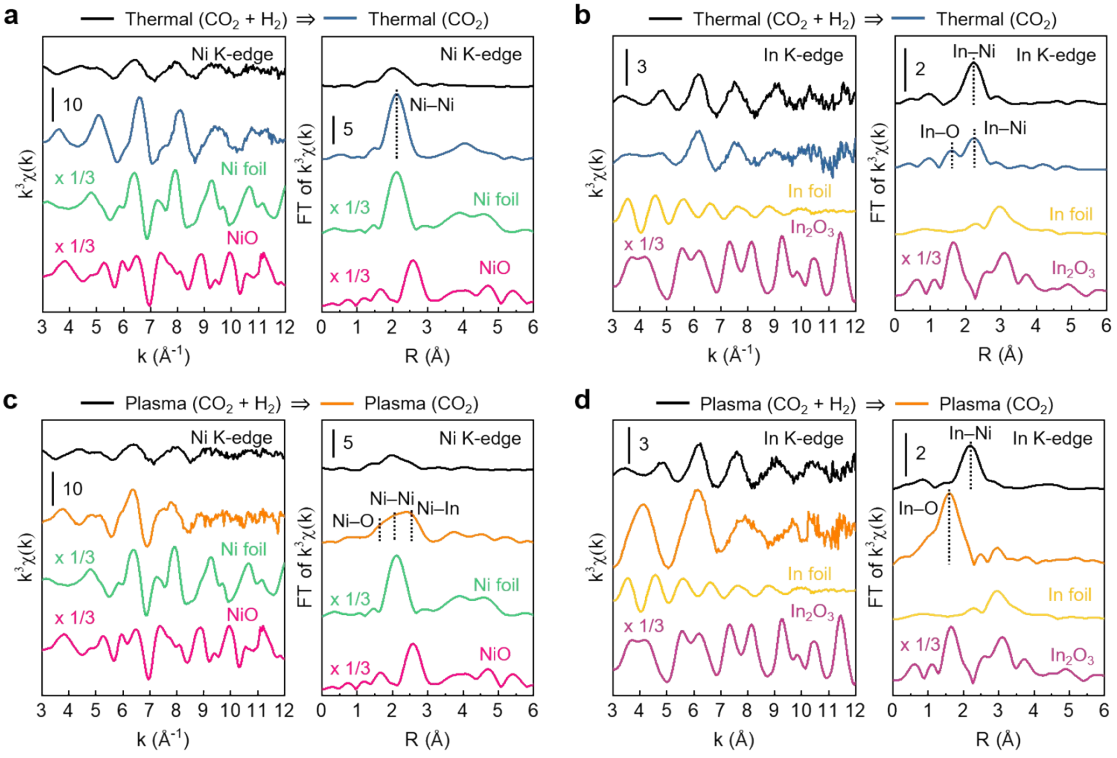

Figure S14. *In situ* Ni and In K-edge EXAFS spectra of Ni–In/Al_2O_3 recorded at 350 °C under (a, b) thermal and (c, d) plasma conditions during CO_2 + H_2 and after switching to CO_2.

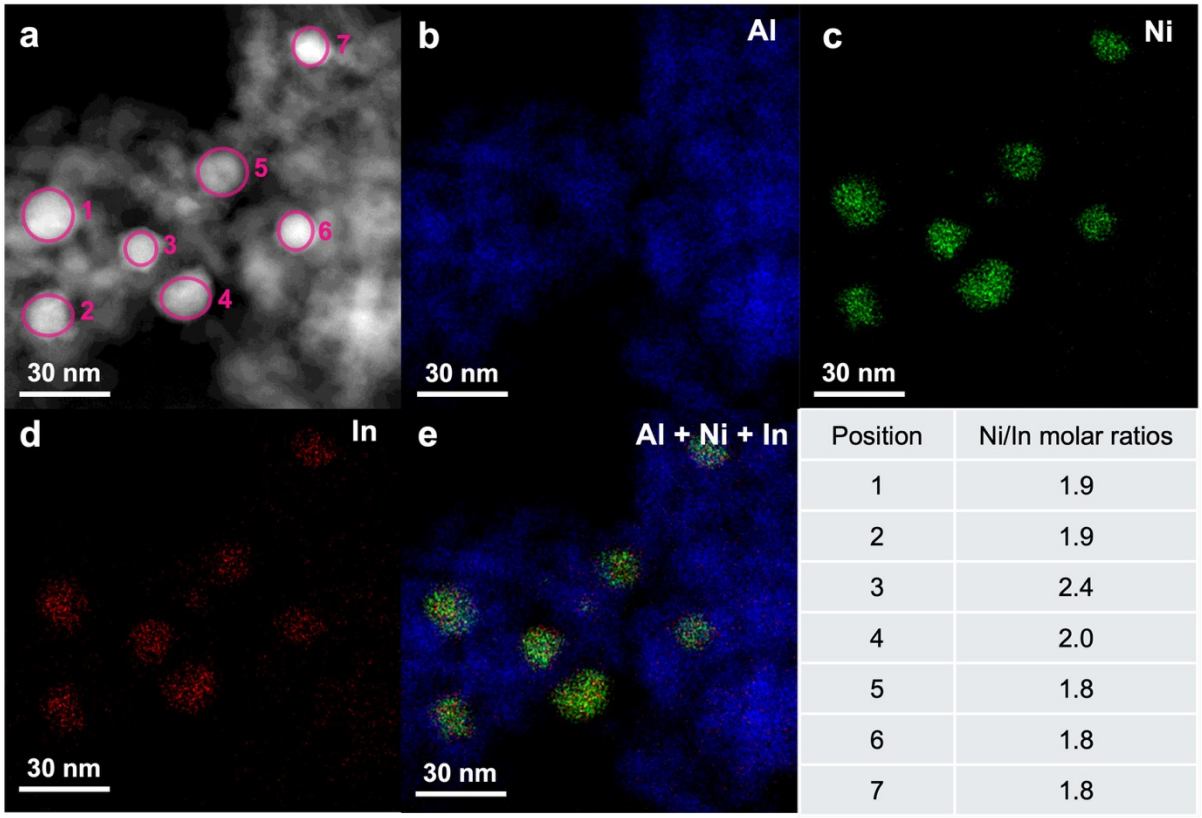

Position	Ni/In molar ratios
1	1.9
2	1.9
3	2.4
4	2.0
5	1.8
6	1.8
7	1.8

Figure S15. TEM analysis of the spent Ni–In/Al_2O_3 catalyst. (a) HAADF-STEM image and corresponding elemental maps of (b) Al, (c) Ni, (d) In, and (e) an overlay of Al, Ni, and In. The Ni/In molar ratios at the positions marked with pink circles in (e) are summarized in the table on the right.

References

1 Z. Sheng, Y. Watanabe, H.-H. Kim, S. Yao and T. Nozaki, *Chem. Eng. J.*, 2020, **399**, 125751.

Fig. 2. Investigation of the reaction mechanism over Ni–In/Al_2O_3. *In situ* TIR spectra recorded at 350 °C during CO_2 exposure under (a) thermal and (b) plasma conditions, and after switching from CO_2 to H_2 under (c) thermal-to-thermal and (d) plasma-to-thermal or plasma conditions.